Radboud Repository

Radboud University Nijmegen

PDF hosted at the Radboud Repository of the Radboud University Nijmegen

The version of the following full text has not yet been defined or was untraceable and may differ from the publisher's version.

For additional information about this publication click this link.
http://hdl.handle.net/2066/75285

Please be advised that this information was generated on 2019-06-18 and may be subject to change.

Modeling and analysis of the three-dimensional current density in sandwich-type single-carrier devices of disordered organic semiconductors

J. J. M. van der Holst,[1,*] M. A. Uijttewaal,[2] B. Ramachandhran,[1] R. Coehoorn,[3,4] P. A. Bobbert,[1] G. A. de Wijs,[2] and R. A. de Groot[2]

[1]*Group Polymer Physics and Eindhoven Polymer Laboratories, Eindhoven University of Technology, P.O. Box 513, 5600 MB Eindhoven, The Netherlands*

[2]*Electronic Structure of Materials, Institute for Molecules and Materials, Radboud University-Nijmegen, Heyendaalseweg 135, 6525 AJ Nijmegen, The Netherlands*

[3]*Philips Research Laboratories-Eindhoven, High Tech Campus 4, 5656 AE Eindhoven, The Netherlands*

[4]*Group Molecular Materials and Nanosystems, Department of Applied Physics, Eindhoven University of Technology, P.O. Box 513, 5600 MB Eindhoven, The Netherlands*

(Received 24 November 2008; published 9 February 2009; corrected 28 April 2009)

We present the results of a modeling study of the three-dimensional current density in single-carrier sandwich-type devices of disordered organic semiconductors. The calculations are based on a master-equation approach, assuming a Gaussian distribution of site energies without spatial correlations. The injection-barrier lowering due to the image potential is taken into account, so that the model provides a comprehensive treatment of the space-charge-limited current as well as the injection-limited current (ILC) regimes. We show that the current distribution can be highly filamentary for voltages, layer thicknesses, and disorder strengths that are realistic for organic light-emitting diodes and, that, as a result, the current density in both regimes can be significantly larger than as obtained from a one-dimensional continuum drift-diffusion device model. For devices with large injection barriers and strong disorder, in the ILC transport regime, good agreement is obtained with the average current density predicted from a model assuming injection and transport via one-dimensional filaments [A. L. Burin and M. A. Ratner, J. Chem. Phys. **113**, 3941 (2000)].

DOI: 10.1103/PhysRevB.79.085203 PACS number(s): 72.20.Ee, 72.80.Le, 72.80.Ng, 85.30.De

I. INTRODUCTION

Organic semiconductors are presently used in a wide variety of devices, such as organic light-emitting diodes (OLEDs),[1] organic field-effect transistors,[2] and organic photovoltaic cells.[3] In these materials, which are often amorphous or near amorphous, an important role is played by disorder: it contributes to the localization of electronic states and strongly influences the hopping rates of the charge carriers between the localized states. Our understanding of devices based on disordered organic semiconductors within which hopping conduction takes place is far less developed than our understanding of transport in devices based on crystalline inorganic semiconductors.

The disorder in organic semiconductors used in OLEDs is often modeled by assuming that the on-site energies are random variables, taken from a Gaussian density of states (DOS). Monte Carlo (MC) simulations of the hopping transport of single carriers (the low carrier-density Boltzmann limit) in a Gaussian DOS were performed by Bässler and co-workers,[4,5] showing a non-Arrhenius temperature dependence $\mu \propto \exp[-c\hat{\sigma}^2]$ of the charge-carrier mobility μ, with $\hat{\sigma} \equiv \sigma / k_B T$, T the temperature, k_B the Boltzmann constant, σ the width of the Gaussian DOS, and c a numerical factor. This work is usually referred to as the Gaussian disorder model (GDM). For the dependence on the electric field, F, a Poole-Frenkel $\mu \propto \exp[\gamma\sqrt{F}]$ behavior was found, in a limited field range, where the factor γ depends on temperature. Gartstein and Conwell[6] pointed out that a spatially correlated potential for the charge carriers is needed to better explain experimental data. These data suggest the existence of Poole-Frenkel behavior in a rather wide region of field strengths. Their work led to the introduction of the correlated disorder model. Several possible causes for this correlation were given, such as the presence of electric dipoles[7,8] or (in the case of polymers) thermally induced torsions of the polymer chains.[9]

For a long time, it has been known that the mobility in disordered inorganic[10] and organic[11] materials is not only a function of the temperature and electric field but also of the carrier density. This dependence has to be accounted for at densities for which state-filling effects are important. The independent-carrier assumption, made in the MC simulations by Bässler and co-workers,[4,5] is then invalid and the mobility increases with increasing carrier density, as the occupation of the deepest states by a certain fraction of the carriers reduces the effect of these states as trapping centers. For the case of a Gaussian DOS, this effect occurs for concentrations (ratio of the carrier density to the site density) larger than $c_{\mathrm{crossover}} = (1/2) \times \exp[-\hat{\sigma}^2/2]$. Schmechel[12] argued that the resulting enhancement of the mobility in a Gaussian DOS could explain the mobility in disordered doped injection layers used in OLEDs, in which the carrier concentrations are very high. Using the results of a computational study of the T, F, and n_h (hole density) dependences of the hopping mobility in a Gaussian DOS, Pasveer *et al.*[13] showed that the effect can even provide a good quantitative explanation for the concentration dependence of the hole mobility and the occurrence of a crossover density, which were discovered experimentally by Tanase *et al.*[14] for hole-only devices based on the undoped semiconducting polymer poly(*p*-phenylenevinylene) (PPV). The experimental

 ©2009 The American Physical Society

temperature-dependent current density versus voltage $[J(V)]$ curves of sandwich-type hole-only devices could be explained without invoking a correlation between the site energies.[13] At room temperature, the density dependence of the mobility was found to be much more important than the electric-field dependence. The version of the GDM presented in Ref. 13, which takes into account both the dependence of the mobility on the carrier density and the electric field, will be called the extended Gaussian disorder model (EGDM).

Coehoorn *et al.*[15] showed that the carrier density and temperature dependence of the mobility obtained from the numerically exact master-equation approach in Ref. 13 are consistent with the results obtained from various existing semianalytical models for transport in disordered materials[11,16,17] and that in other models[18,19] a simple but important correction (to more properly take into account the percolative nature of the transport) is sufficient. The similarity of these models was explained by their common notion of critical hops on a percolating path that determine the size of the current.

In this paper, we investigate the effects of disorder on the transport through complete devices. It is already well known that the percolative nature of the transport in a disordered organic semiconductor leads to a strongly filamentary structure of the current along the percolation paths.[20–24] This raises the question to what extent one-dimensional (1D) continuum drift-diffusion device models, within which the current density is assumed to be laterally uniform, provide accurate predictions of the $J(V)$ curves. It is important to answer this question because such 1D models are numerically much more efficient than complete three-dimensional (3D) device models and are the obvious choice in modeling the complex multilayer structures that will be used in commercial OLEDs. We address this question by making a detailed comparison between the current densities obtained from a full 3D master-equation model for the hopping transport in single-layer single-carrier sandwich-type devices and the current densities obtained from a 1D continuum drift-diffusion device model. The 1D model that we will use is based on the EGDM. It is an extension of an approach introduced in Ref. 25 to include the effective injection-barrier lowering due to the image-potential effect. Earlier work on PPV-based polymers revealed no necessity to take correlated disorder into account,[13] such as is done in the work of Tutiš *et al.*[21] These authors used a master-equation model for calculating the current density in the case of correlated disorder for the situation that the current is limited by injection, taking the image potential into account but neglecting space-charge effects.

We show that the 1D continuum model used in this paper provides for various cases of interest quite accurate predictions of the voltage dependence of the current density. However, we also find a distinct offset of the current for relatively large disorder ($\hat{\sigma}=6$) and a small layer thickness (22 nm). The filamentarity of the current density is then quite pronounced. We present visualizations of the three-dimensional current density and discuss the effects of the filamentary nature of the current density in the case of strong disorder on the current density in the space-charge-limited current (SCLC) and injection-limited current (ILC) transport regimes. Our 3D model will allow us to analyze the appropriateness of various previously proposed models for charge-carrier injection in OLEDs. In view of the focus, in a large part of this paper, on the issue of charge-carrier injection, we give in the remainder of this introduction a brief review of these models.

Within the simplest approach to the problem of carrier injection and subsequent transport in organic semiconductor devices it is assumed that the charge carriers in the organic semiconductor at the contact are in thermal equilibrium with the electrons in the metal electrode. The presence of an injection barrier, Δ, then reduces the density of carriers at the contact with the metal, n_c, to a value given by $n_c=N_t/[1+\exp(\Delta/k_BT)]$, with N_t the total density of molecular sites. Here, Δ is defined as the (positive) energy difference between the Fermi energy in the metal and the energy of the highest occupied molecular orbital or lowest unoccupied molecular orbital states in the semiconductor. The current density is obtained by self-consistently solving the drift-diffusion equation, taking the space charge in the device into account and using n_c as a fixed boundary condition. For the case of a constant mobility and diffusion coefficient, this boundary-value problem can be solved analytically.[26] In a symmetric device (equal left and right contacts) the current density is then injection limited if $n_c \approx n_0 \equiv \epsilon k_BT/(e^2L^2)$ or smaller, with ϵ the dielectric constant, e the elementary charge, and L the device thickness. For $L=100$ nm, $N_t=10^{27}$ m^{-3}, and a relative dielectric constant $\epsilon_r=3$ (a typical device), the injection-limited transport regime therefore sets in (at room temperature) around $\Delta \approx 0.4$ eV. For larger injection barriers, the space charge in the device can be neglected and the carrier density is uniform and equal to n_c. The injection-limited current density is then given by $J_{\mathrm{ILC}}=en_c\mu V/L$.

For two reasons the problem of carrier injection in organic semiconductors is more complicated than assumed in the model discussed above. First, the model neglects the image-charge interaction between an individual charge and its image charge in the electrode. In the SCLC regime, the image-charge effect is to a certain extent taken into account by self-consistently solving the Poisson equation for the *layer-averaged* charge density. In that regime, the resulting error is small. However, in the ILC regime the *actual* injected charge at a specific site associated with one carrier is one electronic charge at that site, which is much larger than the layer-averaged charge at sites in the same layer. The effect of the image potential on the current density in the ILC regime has been studied by Emtage and O'Dwyer,[27] and more recently by Scott and Malliaras[28] and by Masenelli *et al.*[29] Effectively, it leads to a lowering of the effective injection barrier with increasing voltage.

Second, all models discussed so far neglect the effects of energetic disorder. Its relevance to the injection process in OLED-type devices was first noted by Gartstein and Conwell,[30] who studied the combined effects of the image potential and the Gaussian disorder in the ILC regime using a MC simulation. These authors showed that disorder can give rise to a strongly enhanced field dependence of the injection-limited current density. Arkhipov *et al.*[31] developed a semianalytical 1D approach to this problem. For relatively

high temperatures and small disorder good agreement was found with the results of MC calculations.[32] As a result of the injection in tail states, the ILC in a material with a Gaussian DOS was predicted to be larger than the ILC in an ordered material, for a given value of Δ, and its decrease with decreasing temperature was predicted to be smaller. The latter effect was confirmed by van Woudenbergh *et al.*[33] from an experimental study of the ILC in PPV-based devices. Burin and Ratner (BR) (Ref. 34) studied this problem by assuming that for sufficiently high field strengths and in the ILC regime the injection and transport occur through 1D straight paths, effectively lowering the injection barrier. Recently, support for the latter model has been obtained from a measurement using electric-force microscopy of the potential drop near the injecting contacts in a lateral two-terminal metal/organic/metal device.[35] As noted already by the authors,[32] it is expected that the Arkhipov model underestimates the stochastic nature of the carrier motion in the vicinity of the barrier, when at high fields only a few rare easy pathways dominate the current density. On the other hand, the BR model will overrate this effect, in particular for relatively small fields, when more easy nonlinear trajectories are neglected. These weaknesses of the Arkhipov and BR models are confirmed by the 3D modeling results presented in this paper.

The paper is built up as follows. Sections II A and II B discuss the 3D master-equation method and the 1D continuum model, respectively, used for calculating the current density in single-carrier devices. In Sec. III we present the results of the 3D master equation and 1D continuum modeling of the voltage dependence of the current density. In Sec. IV we investigate the 3D structure of the current distribution and discuss the consequences of this structure for the validity of different models: our 1D continuum model, the BR model, and the Arkhipov model. Section V contains a summary and conclusions.

II. THEORY AND METHODS

A. Three-dimensional master-equation model

In this section the 3D master-equation method is described for calculating the current density in single-carrier devices, consisting of a single organic layer that is sandwiched in between two metallic electrode layers. The device is modeled as a three-dimensional cubic $m_x \times m_y \times m_z$ lattice with an intersite distance a. Lattice sites will be denoted by $\mathbf{i} \equiv \{i_x, i_y, i_z\}$. The applied field is directed along the x axis, and the planes formed by the sites at $i_x = 1$ and $i_x = m_x$ are viewed as the metallic injecting and collecting electrode planes, respectively. The sites at all other planes will be called "organic sites." Along the lateral (y and z) directions periodic boundary conditions are applied. Every site represents a localized state and the carrier occupation probability on a site $\mathbf{i}$ will be denoted by $p_\mathbf{i}$.

We assume that conduction in the organic semiconductor takes place by hopping of charge carriers from one localized site to another, as a result of a tunneling process that is thermally assisted due to the coupling to a system of acoustical phonons. This leads to a hopping rate from site $\mathbf{i}$ to $\mathbf{j}$ of the Miller-Abrahams form[36]

$$W_{\mathbf{ij}} = \nu_0 \exp\left[-2\alpha R_{\mathbf{ij}} - \frac{E_\mathbf{j} - E_\mathbf{i}}{k_B T}\right] \quad \text{for} \quad E_\mathbf{j} \geq E_\mathbf{i}, \tag{1a}$$

$$W_{\mathbf{ij}} = \nu_0 \exp[-2\alpha R_{\mathbf{ij}}] \quad \text{for} \quad E_\mathbf{j} < E_\mathbf{i}, \tag{1b}$$

where ν_0 is an intrinsic rate, $R_{\mathbf{ij}} \equiv |\mathbf{R_j} - \mathbf{R_i}|$ is the distance between sites $\mathbf{i}$ and $\mathbf{j}$, α is the inverse localization length of the localized wave functions, and $E_\mathbf{i}$ is the energy of the state at site $\mathbf{i}$. For simplicity, we assume that the hopping rates from the electrode sites to the organic sites and vice versa are given by the same expression [Eq. (1)] as the rates for the mutual hopping between organic sites. It is to be expected that the specific rate taken for the hopping between the electrode sites and the sites in the first and last organic layers has almost no influence on the final current-voltage characteristics of the device, as long as this hopping rate is large enough to establish equilibrium between these sites.

In this paper only symmetric devices are considered, i.e., devices with equal injection barriers, Δ, at the injecting and collecting electrodes, but our methods can just as well be applied to asymmetric devices. The injection barrier is defined as the distance in energy between the Fermi level in the electrode and the top of the Gaussian DOS. The energy of each organic site is therefore equal to the sum of a random on-site contribution, drawn from a Gaussian DOS with a width equal to σ, and an offset due to the injection barrier,

$$g(E) = \frac{1}{\sqrt{2\pi\sigma a^3}} \exp\left[-\frac{(E-\Delta)^2}{2\sigma^2}\right], \tag{2}$$

plus the electrostatic energy contributions $e\Phi_\mathbf{i}$ and $e\Phi_{\mathrm{im},\mathbf{i}}$ due to the applied field and the space charge and due to the image-charge effect, respectively. The Fermi energy in the collecting electrode is taken as the zero-energy reference value, so that the electrostatic potentials at the two electrode planes are given by $e\Phi(i_x = 1) = eV$ and $e\Phi(i_x = m_x) = 0$, where V is the applied driving voltage (bias). The contribution to the electrostatic potential due to the space charge is calculated using the Poisson equation from the laterally averaged charge-carrier density in each layer i_x. As a consequence of this approximation, $e\Phi_\mathbf{i}$ depends only on the layer index i_x. Also the image-charge contribution depends only on the distance of the site to each of the electrodes. It is given by

$$e\Phi_{\mathrm{im}}(i_x) = -\frac{e^2}{16\pi\epsilon_0\epsilon_r a}\left(\frac{1}{m_x - i_x} + \frac{1}{i_x - 1}\right) \tag{3}$$

at the organic sites. Here e is the unit charge, ϵ_0 the vacuum permeability, and ϵ_r the relative dielectric constant of the organic material. There is no image-charge contribution at the electrode sites. Equation (3) is the first-order term in an expansion in which repetitive images are taken into account.[37] For the device thicknesses considered, no significant change of the results was obtained when taking higher-order images into account.

The occupational probabilities $p_\mathbf{i}$ for the organic sites are obtained by solving the Pauli master equation

$$\frac{\partial p_{\mathbf{i}}}{\partial t} = -\sum_{\mathbf{j}\neq\mathbf{i}, j_x\neq 1, m_x} [W_{\mathbf{ij}} p_{\mathbf{i}}(1-p_{\mathbf{j}}) - W_{\mathbf{ji}} p_{\mathbf{j}}(1-p_{\mathbf{i}})] - \sum_{\mathbf{j}\neq\mathbf{i}, j_x=1, m_x} [W_{\mathbf{ij}} p_{\mathbf{i}} - W_{\mathbf{ji}}(1-p_{\mathbf{i}})] = 0, \quad (4)$$

where the first sum is related to hopping between organic sites and the last term to hopping from and to the electrodes. The factors $1-p_{\mathbf{i}}$ in this first sum account, in a mean-field approximation, for the fact that only one carrier can occupy a site due to the high Coulomb penalty for the presence of two or more carriers. The second sum describes the hopping from sites of the outermost organic layers to the electrode sites (first term between square brackets) and the hopping from electrode sites to the outermost organic layers (second term), where we assume that there are always charges on the electrode sites ready to hop to the organic sites and that the electrode sites can always accept a charge from the organic sites. We take into account hopping over a maximum distance of $\sqrt{3}a$, which is sufficient for the values of a and α that we will consider (see Sec. III).

In order to solve the Pauli master equation for the occupational probabilities $p_{\mathbf{i}}$, we use an iterative procedure similar to the one described in Refs. 13 and 20. From these occupational probabilities we can calculate the current through the device. At each organic site $\mathbf{i}$, we define a local particle current $J_{p,\mathbf{i}}$ in the direction of the collecting electrode

$$J_{p,\mathbf{i}} = \sum \{W_{\mathbf{ij}} p_{\mathbf{i}}(1-p_{\mathbf{j}}) - W_{\mathbf{ji}} p_{\mathbf{j}}(1-p_{\mathbf{i}})\}, \quad (5)$$

where the summation is over all sites $\mathbf{j}$ for which $j_x > i_x$. The total electrical current density is then given by

$$J = \frac{1}{m_y m_z} \sum \frac{e J_{p,\mathbf{i}}}{a^2}, \quad (6)$$

where the summation is over all $m_y \times m_z$ sites within any plane parallel to the electrodes within the device.

As the electrostatic potential is determined by the charge distribution, whereas the charge distribution can only be calculated if the potential is known, both should be determined self-consistently. To obtain the self-consistent solution we use the following iteration procedure:

(1) Start with a potential Φ that linearly decreases from injecting to collecting electrode.

(2) Solve the master equation, Eq. (4).

(3) Update the electrostatic potential, which has changed due to the change of the space charge.

(4) Recalculate all the hopping rates $W_{\mathbf{ij}}$ using Eq. (1).

If the total charge and the current in the device have converged, the procedure stops, otherwise the procedure starts again at the second step.

B. One-dimensional continuum model

We will compare the $J(V)$ curves obtained from the 3D master-equation model discussed in Sec. II A to the $J(V)$ curves obtained from a 1D continuum drift-diffusion model. The current density in this model is given by

$$J = n(x) e \mu(x) F(x) - e D(x) \frac{dn(x)}{dx}, \quad (7)$$

where $n(x)$ and $F(x)$ are the local charge-carrier density and electric field, respectively, which are related by the Poisson equation, $dF/dx = (e/\epsilon) n(x)$. The dependence of the local mobility, $\mu(x) = \mu[T, n(x), F(x)]$, on the temperature, the charge-carrier density, and the electric field is taken from the parametrization given for the EGDM in Ref. 13. The local diffusion coefficient, $D(x)$, is obtained from the local mobility by using the generalized Einstein equation.[38] We note that the expressions given in Ref. 13 for the mobility within the EGDM were obtained from essentially the same 3D master-equation model as discussed above, but then for a system with a uniform carrier density and electric field and including also periodic boundary conditions along the x direction. Therefore, any difference between both approaches will be exclusively due to a failure of taking the actual nonuniform 3D current density into account in the 1D model.

For efficiently solving the 1D drift-diffusion-Poisson problem within the EGDM, we have used an extended version of the numerical method described recently by van Mensfoort and Coehoorn.[25] Within the standard form of that method, described in Ref. 25, the carrier densities at the electrode planes are assumed to be constant (voltage independent) and given by the condition of local thermal equilibrium between the metal and the organic layer. The density of carriers at the contact with the metal, n_c, is then given by

$$n_c = \int_{-\infty}^{\infty} \frac{g(E)}{1+\exp[E/(k_B T)]} dE, \quad (8)$$

with the DOS $g(E)$ given by Eq. (2). When the injection barrier is sufficiently small, the large carrier density in the organic layer near the injecting electrode will give rise to a local drift contribution of the particle current toward the injecting electrode. Under these conditions, the electrostatic field near the interfaces is the result of a net electrostatic interaction that is the overall sum of the individual contributions from the charges and image charges of many electrons. The standard 1D model treats this in a fair way, viz., by solving the 1D Poisson equation assuming a laterally homogeneous charge density. On the other hand, when the injection barrier is sufficiently large, so that the local drift contribution to the particle current is directed away from the injecting electrode, the predominant contribution to the electrostatic field near the electrode is due to the image charge of the injected carrier itself. In order to be able to account for such cases, we have extended the 1D model presented in Ref. 25 by making use of an image-charge-corrected barrier height of the form first suggested by Emtage and O'Dwyer,[27]

$$\Delta' = \Delta - e\sqrt{\frac{eF_c}{4\pi\epsilon_0\epsilon_r}}, \quad (9)$$

with F_c the (positive) electric field at the contact plane. F_c and Δ' are determined self-consistently using an iterative procedure. When $F_c < 0$, the full injection barrier Δ is used. We show in Sec. III that this method of taking the image-charge potential into account in 1D calculations of $J(V)$

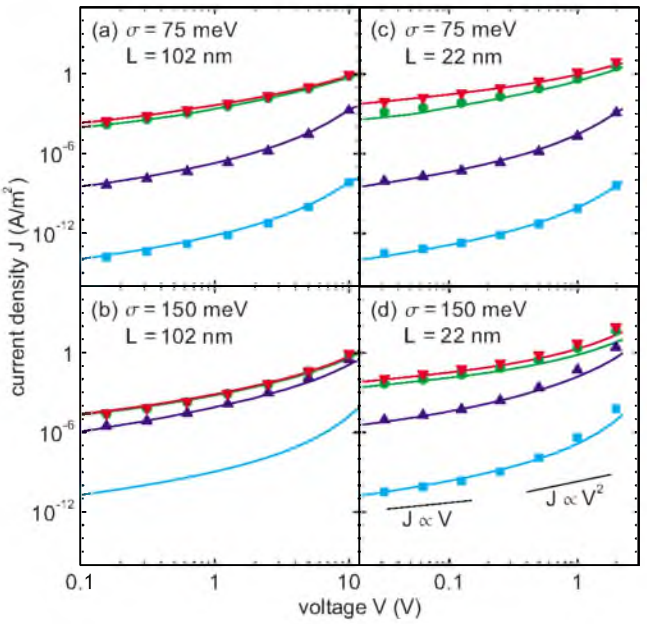

FIG. 1. (Color online) Dependence of the current density (J) on the driving voltage (V) for devices with thicknesses of $L=102$ and 22 nm and disorder strengths of $\sigma=75$ and 150 meV, as indicated in (a)–(d). The results are for room temperature and lattice constant $a=1.6$ nm. The values used for the attempt-to-jump frequency, ν_0, are 3.5×10^{13} s^{-1} for devices with $\sigma=75$ meV and 1.4×10^{16} s^{-1} for devices with $\sigma=150$ meV. These values correspond to a mobility prefactor μ_0 (as defined in Ref. 13) equal to 4.8×10^{-14} and 1.1×10^{-16} m^2/V s, respectively. Symbols: results obtained from the 3D master-equation approach for different injection barriers Δ: 0 eV (downwards pointing triangles), 0.33 eV (circles), 0.67 eV (upwards pointing triangles), and 1 eV (squares). In (b) no converged master-equation results for $\Delta=1$ eV could be obtained. Solid lines: results obtained from the 1D continuum drift-diffusion model as explained in the main text.

curves leads to a surprisingly good agreement with the results of the 3D master-equation model, provided that the transport is well in the ILC regime.

III. RESULTS

In Fig. 1 we display the room-temperature current density as a function of applied voltage, as obtained from the 3D and 1D calculations described in Sec. II. The results are given for different injection barriers, Δ, equal to 0, 0.33, 0.67, and 1 eV. The lattice constant has been taken equal to $a=1.6$ nm, a value found in Ref. 13 from modeling the transport in a hole-only device based on the PPV derivative OC_1C_{10}-PPV (poly[2-methoxy-5-(3′,7′-dimethyloctyloxy)-*p*-phenylene vinylene]). The four plots show the results for two values of the dimensionless disorder parameter, $\hat{\sigma}=3$ and 6, corresponding to $\sigma=75$ and 150 meV at room temperature, respectively, and for two layer thicknesses L, indicated in the figures as 22 and 102 nm. The actual thicknesses are 13 layers (22.4 nm) and 63 layers (102.4 nm), respectively. The attempt-to-jump frequency, ν_0, is chosen such that at vanishing injection barrier, the current density as obtained from the 3D model is equal to 1 A/m^2 at $V=10$ V for the 102 nm devices. This value of ν_0 and the corresponding values of the mobility at zero field in the low-density Boltzmann limit used within the 1D-model calculations are given in the figure caption and will be used throughout the rest of the paper. Like in Ref. 13, we take the wave-function decay length, α^{-1}, equal to $a/10$. The lateral grid size is 50×50 sites. The relative accuracy of the results is approximately 10%, which was concluded by carrying out calculations for different lateral grid sizes and disorder realizations.

A remarkably good agreement is obtained between the 3D master-equation results (symbols) and the 1D continuum-model results (lines), except for the thin ($L=22$ nm) device with strong disorder ($\sigma=150$ meV) at voltages exceeding 1 V [Fig. 1(d)]. For the lowest injection barriers, $\Delta=0$ and 0.33 eV, the devices are in the SCLC regime and the current is almost independent of the size of the injection barrier. At small voltages, the current-voltage curves are linear (ohmic), as expected when the transport is predominantly due to charge-carrier diffusion.[25] The slope of the current-voltage curve (on a double-log scale) increases with increasing voltage, eventually to a value that exceeds the value of two that would be obtained for the case of a constant mobility in the presence of a drift contribution only (Mott-Gurney relationship). This can be viewed as a result of the carrier-density dependence and the electric-field dependence of the mobility.[13,25] When the injection barrier increases the ILC regime is entered and the voltage dependence becomes much more pronounced. For high injection barriers the current in the 22 and 102 nm devices is almost the same for equal injection barriers if the voltage is scaled with the device thickness. For the case of $\sigma=75$ meV this happens for injection barriers $\Delta=0.67$ and 1 eV. For the case of $\sigma=150$ meV, space-charge effects are still dominant at an injection barrier of $\Delta=0.67$ eV, the reason being that a higher value of σ leads to a higher carrier density at the interface than for $\sigma=75$ meV (the tail states of the Gaussian DOS are filled to a larger extent), and hence to stronger limitation of the current by space-charge effects. We remark that because of convergence problems we were not able to obtain master-equation results for $\Delta=1$ eV for the 102 nm device.

We analyze the situation in more detail with the help of Fig. 2, which shows a comparison of the calculated injection-barrier dependent current density in the 22 nm devices at a bias of 2 V and room temperature as obtained from the 3D master-equation approach and as obtained from various other approaches, for $\sigma=75$ meV [Fig. 2(a)] and $\sigma=150$ meV [Fig. 2(b)]. We first focus on the results in the SCLC regime. For very small values of Δ, the 1D calculations were carried out without taking the image-charge effect into account since the field is then directed toward the injecting electrode ($F_c<0$ as explained in Sec. II B). Calculations including the image-charge effect were only carried out for $\Delta>0.20$ eV and $\Delta>0.35$ eV for $\sigma=75$ and 150 meV, respectively, as indicated by the arrows in Fig. 2. For these cases the inclusion of the image potential leads to an effective barrier *decrease* [Eq. (9)]. Actually, for smaller values of Δ the inclusion of the image potential would lead to a small effective barrier *increase*, due to charge trapping in the potential well near the interface, deepened by the image potential. As a

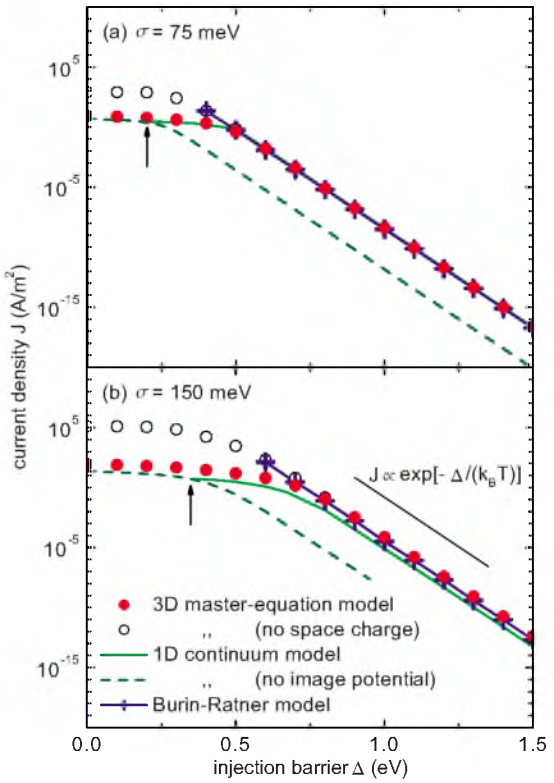

FIG. 2. (Color online) Dependence of the current density (J) on the injection barrier (Δ) for different models. The displayed results are for devices with disorder strengths of (a) $\sigma=75$ and (b) $\sigma=150$ meV, device thickness $L=22$ nm, driving voltage $V=2$ V, room temperature, and lattice constant $a=1.6$ nm. The other parameters are the same as in Fig. 1. Arrows indicate the points where the electric field at the injecting electrode switches sign within the 1D continuum model.

result, the actual current density would be smaller than as predicted from the 1D model used here. One may estimate the effect by extrapolating the 1D current-density curve as obtained with the image potential to $\Delta=0$ eV. The extrapolated current density is a factor of ~ 1.5 and ~ 4.5 smaller than the 1D current density given in Fig. 2 for the cases $\sigma=75$ and 150 meV, respectively. For $\sigma=75$ meV the agreement between the 3D master-equation and 1D continuum-model results is very good, with an underestimation of the current density by the 1D continuum model in the SCLC regime by only a factor of about 2. However, for $\sigma=150$ meV the 1D continuum model underestimates the current density in the SCLC regime by a factor of about 4. We note that the extrapolated current densities mentioned above, including the image potential, yield a stronger underestimation of the current densities in the SCLC regime. We may thus conclude that the omission of the image potential in the 1D continuum model accidentally corrects part of an intrinsic underestimation of the current density by the 1D model. In Sec. IV, we will investigate the origin of this underestimation.

With increasing injection barrier we see in Fig. 2 a transition from the SCLC to the ILC regime, with finally an Arrhenius behavior, $J \propto \exp[-\Delta/k_B T]$ of the current density. In the ILC regime the inclusion of the image potential is of crucial importance, which can be seen from the continuation of the 1D continuum-model calculations without image potential (dashed lines), which predict a far too low current. For $\sigma=75$ meV the agreement between the 3D master-equation and the 1D continuum-model results in the ILC regime is excellent. For $\sigma=150$ meV the 1D continuum model underestimates the current density in the ILC regime by a factor of about 8. The origin of the underestimation of the current density by the 1D model in the SCLC and ILC regimes is investigated in Sec. IV.

IV. THREE-DIMENSIONAL STRUCTURE OF THE CURRENT DISTRIBUTION: CONSEQUENCES FOR DIFFERENT MODELS

In order to obtain a better insight in the effects that cause the discrepancies between the 3D master-equation and the 1D continuum-model results, we have studied the three-dimensional structure of the current distribution. Figure 3 shows the room-temperature current-density distribution for the 22 nm device at a bias of $V=2$ V, an injection barrier $\Delta=1$ eV, for $\sigma=75$ [Figs. 3(a) and 3(b)] and $\sigma=150$ meV [Figs. 3(c) and 3(d)]. Figures 3(a) and 3(c) show the current distribution as viewed from the side, whereas Figs. 3(b) and 3(d) show views from the injecting to the collecting electrode. The local current density has been calculated by summing for each site in a box of $13\times50\times50$ sites the net currents to the nine sites in the adjacent layer to which we allow hopping and attributing this sum to this site, according to Eq. (5). We have used the same disorder realization for $\sigma=75$ and 150 meV, apart from an obvious factor of 2. The figures reveal that the current density is strongly filamentary for $\sigma=150$ meV and already weakly filamentary for $\sigma=75$ meV. Such filamentary structures in the current distribution have been reported before[20–24] and are caused by percolation effects, which increase with increasing disorder. We have also investigated the current distributions for zero injection barrier and found a less pronounced but still clear filamentary structure, showing that this structure is enhanced by the injection barrier, but that its existence does not require a finite injection barrier.

Clearly, the filamentary structure of the current distribution means that almost all the current flows through a relatively small number of sites. Since the 1D continuum model is based on the EGDM, in which the *bulk* effects of the filamentary structure of the current have been properly taken into account,[13] it can be expected that the 1D continuum model works properly for thick devices. Indeed, Figs. 1(a) and 1(b) shows that for the device with $L=102$ nm device the agreement between the 3D master-equation and 1D continuum-model results is very good. As long as the typical length scale of the spatial structure of the current distribution is small compared to the device thickness, one can speak about a "local" mobility that can successfully be used in 1D continuum models. However, for devices with a thickness of the order of or smaller than this typical length scale, the concept of a local mobility breaks down.[23] The presence of current filaments from the injecting to the collecting electrode then leads to a *higher* net current than obtained with a

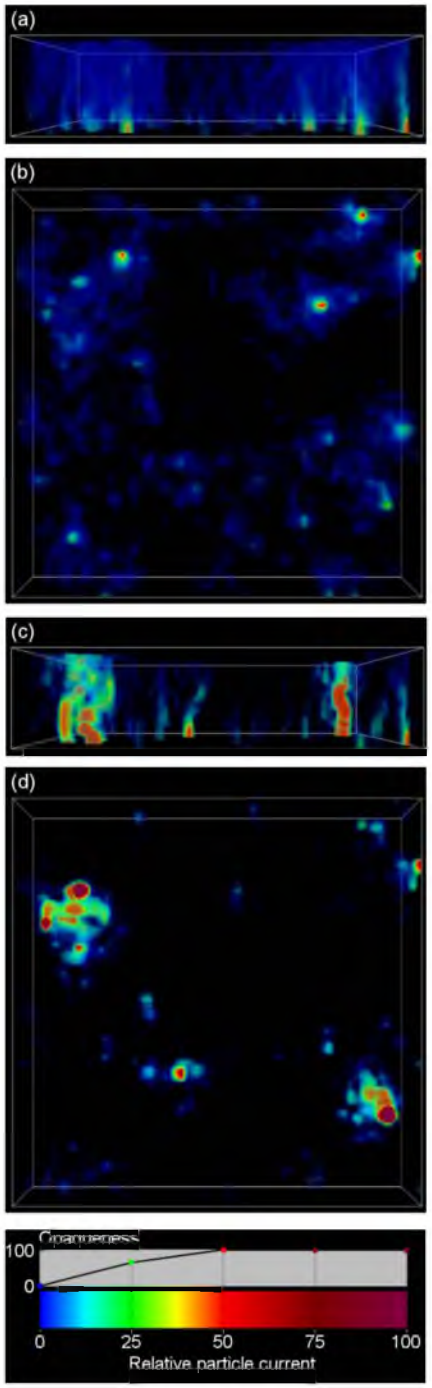

FIG. 3. (Color online) Three-dimensional representation of the relative local current density, given by $J_{\mathrm{rel},\mathbf{i}}=J_{\mathbf{i}}/J_{\mathrm{av}}$, with $J_{\mathbf{i}}$ the absolute local current density given by Eq. (5) and J_{av} the average local current density in the device. The displayed results are for devices with disorder strengths of [(a) and (b)] $\sigma=75$ meV and [(c) and (d)] $\sigma=150$ meV, device thickness $L=22$ nm, driving voltage $V=2$ V, injection barrier $\Delta=1$ eV, room temperature, and lattice constant $a=1.6$ nm. In (a) and (c) the device is viewed from the side with the injecting electrode at the bottom, whereas (b) and (d) give views from the injecting to the collecting electrode. The local current density is coded with a color and transparency, with the coding scheme indicated at the bottom. The lateral grid size used is 50×50 sites. The boundaries of the device are depicted by a white bounding box.

1D continuum model; the effect becoming larger for larger electric field. This is the reason for the discrepancies found in Figs. 1(d) and 2(b) found for $L=22$ nm and $\sigma=150$ meV between the 3D master-equation and 1D continuum-model results, both in the SCLC and ILC regimes. Indeed, one can see from Fig. 3 that the typical length scale of the structures in the current distribution is roughly of the order of 10 nm. Since the filamentary structure is less pronounced for smaller disorder, the agreement between the 3D master-equation and 1D results in Figs. 1(c) and 2(a) found for $\sigma=75$ meV is much better.

In the remainder of this section, we discuss to what extent the filamentary nature of the current density in the ILC regime is properly taken into account in the Burin-Ratner model[34] and the Arkhipov model.[31] The above point of view about the underestimation of the current by the 1D continuum model is supported by an analysis of the current density using the BR model.[34] Within that model, it is assumed that the total current is a simple sum of independent contributions from linear (one-dimensional) filaments that start at all injecting sites. These contributions can be obtained by solving a 1D master equation for a chain of sites with random Gaussian disorder. We have used the exact solution for the contribution to the current density from a filament at the point (i_y,i_z), given by Eq. 5 in Ref. 34

$$J(i_y,i_z)=\frac{\exp\left(-\frac{e\Delta}{k_BT}\right)}{\exp\left(-\frac{e\Delta}{k_BT}\right)+2\sum_{i_x=2}^{m_x-1}\exp\left(\frac{E(i_x)-eai_xF+e\Phi_{\mathrm{im}}(i_x)}{k_BT}\right)}J_0, \tag{10}$$

with the energies $E(i_x)$ taken randomly from a Gaussian DOS with width σ and with $\Phi(i_x)$ the image potential at site i_x, given by Eq. (3). In contrast to the original expression in Ref. 34 this expression takes into account the finite thickness of the device. The current density is expressed relative to J_0, defined as

$$J_0\equiv\frac{e\nu_0}{a^2}\exp[-2\alpha a], \tag{11}$$

which is the current density that would be obtained from a master-equation calculation for a system with all sites fully occupied ($p_{\mathbf{i}}=1$), in the large-field limit, neglecting the $(1-p_{\mathbf{i}})$ factors that prohibit double occupation [cf. Eq. (4)]. The total current density is then obtained by averaging the contributions from a sufficiently large number of points (i_y,i_z). These contributions are obtained by applying Eq. (10) repeatedly for a large ensemble of random sets of energies $E(i_x)$ and are thus assumed to be uncorrelated. The assumption of 1D filaments, made within the BR model, is consistent with the observation in Fig. 3 of straight filaments close to the injecting electrode. We note that Eq. (10) is derived by assuming instead of the Miller-Abraham hopping rate Eq. (1b) a hopping rate

$$W_{ij} = \frac{\nu_0}{1 + \exp\left[\frac{E_j - E_i}{k_B T}\right]}. \quad (12)$$

We checked that the differences between the two hopping rates only lead to minor differences in the final results.

The current density as predicted from the BR model is indicated in Fig. 2 (line with plusses). For $\Delta > 0.8$ eV, the model provides a quite good approximation to the results of the full 3D master-equation results for large disorder ($\sigma = 150$ meV), so that it may be concluded that the discrepancy with the 1D continuum-model results for large injection barriers is indeed the consequence of a neglect of transport via rare very easy pathways. Figure 2 also shows that the BR model predicts a too high current density for injection barriers smaller than ≈ 0.5 and ≈ 0.7 eV for $\sigma = 75$ meV and $\sigma = 150$ meV, respectively. This may be attributed to the fact that the BR model neglects the effects of space charge, as may be concluded from the results of the 3D master-equation calculations with the space-charge potential switched off (Fig. 2, open circles), which follow the BR results to lower values of Δ.

Another consequence of the filamentary nature of the current density is the occurrence of a statistical variation of the total current through a given surface area. As an example, Fig. 4 shows the distributions of the current density through 80×80 nm^2 devices (i.e., 50×50 sites) of the type studied in Fig. 3, for $\Delta = 1$ eV, and with $\sigma = 75$ meV [Fig. 4(a)] and $\sigma = 150$ meV [Fig. 4(b)], obtained from 3D master-equation calculations (light-gray bars) and from the BR model (black bars). For $\sigma = 75$ meV, the statistical variations are moderate. The width of the distributions is limited to approximately 40% of the average current density. The BR distribution is clearly shifted to smaller current densities as compared to the master-equation distribution. We attribute this to the limitation to one dimension of hops in the BR model, which leads to lower currents than when 3D hopping is allowed. For $\sigma = 150$ meV, the statistical variations are very large. The width of the distributions is comparable to the peak current density, and the strongly asymmetric distributions give rise to an average current density that is equal to more than twice the peak current densities (note the log scale for the x axis). The relative shift of the BR distribution to smaller current densities is significantly larger than for $\sigma = 75$ meV.

Whereas the BR model yields already at the relatively high fields considered in Fig. 2 (10^8 V/m) current densities that are lower than the 3D master-equation results, it may be expected that the model breaks down even more clearly at small fields. Trajectories containing side jumps are then expected to yield even more important contributions to the current density. This is confirmed by the results given in Fig. 5. For devices with $\sigma = 75$ meV, the figure displays the electric-field dependence of the injection-limited current density as obtained from the 3D master-equation model, the 1D-continuum model, the BR model, and the Arkhipov model (discussed later in this section). The injection barrier is $\Delta = 1$ eV. The temperature is varied from 300 to 150 K, corresponding approximately to $\hat{\sigma} = 3$ and $\hat{\sigma} = 6$, respectively. It has already been established from Fig. 1 that the voltage

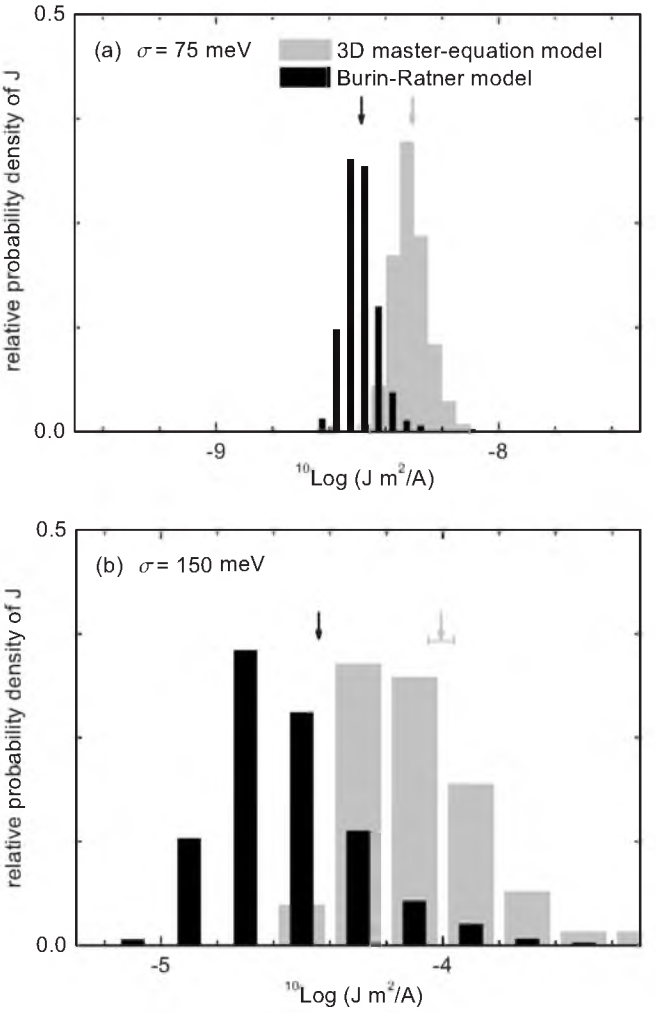

FIG. 4. Probability distribution of the current density J. The displayed results are for devices with disorder strengths of (a) $\sigma = 75$ meV and (b) $\sigma = 150$ meV, device thickness $L = 22$ nm, driving voltage $V = 2$ V, room temperature, lattice constant $a = 1.6$ nm, and injection barrier $\Delta = 1$ eV. The lateral grid size is 50×50 sites. Equally sized bins on a logarithmic scale have been used and the normalization is such that the sum of the lengths of the bars is equal to 1. Light-gray bars: results obtained from the 3D master-equation model. Black bars: results obtained from the Burin-Ratner model. For devices with disorder strength of $\sigma = 75$ (150) meV, 656 (62) samples were used for the 3D master-equation model and 3200 (6400) samples for the Burin-Ratner model. Arrows indicate the corresponding average current densities, which could be very accurately determined, except for the master-equation result for $\sigma = 150$ meV, where an error bar indicates the uncertainty.

dependence of the current density as obtained from the 1D continuum model is in fair agreement with the results from the 3D master-equation model. Therefore, we regard these results (solid curves) as a benchmark. The figure shows that the BR model underestimates the current density at small fields. This indeed suggests that at smaller fields, nonlinear trajectories, which are neglected within the BR model, contribute significantly to the current density.

The 1D continuum model yields the following expression for the current density in the ILC regime:

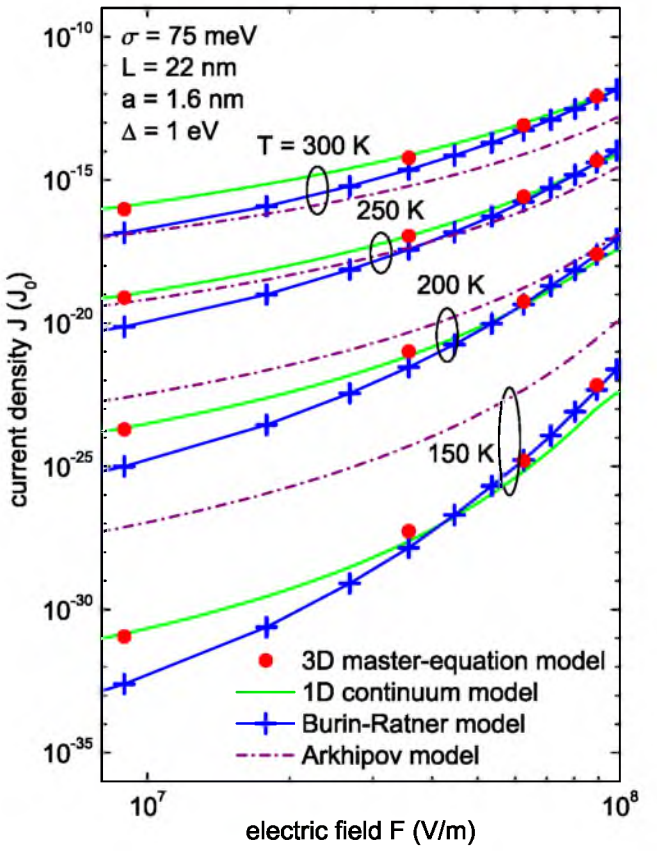

FIG. 5. (Color online) The current density [J in units of J_0 as given by Eq. (11)] as function of the electric field (F) for different temperatures and four different models.

$$J = en_c\mu(n_c,F)F \cong \frac{e}{a^3}\exp\left[-\frac{e\Delta'(F)}{k_BT}+\frac{1}{2}\hat{\sigma}^2\right]\mu(0,F)F$$
$$= \frac{e}{a^3}\exp\left[-\frac{e\Delta'(F)}{k_BT}+\frac{1}{2}\hat{\sigma}^2\right]\frac{a^2\nu_0 ec_1}{\sigma}\exp(-c_2\hat{\sigma}^2)\frac{\mu(0,F)}{\mu(0,0)}F$$
$$\cong \exp\left[-\frac{e\Delta'(F)}{k_BT}+\left(\frac{1}{2}-c_2\right)\hat{\sigma}^2\right]f(F)\frac{eaF}{\sigma}J_0, \quad (13)$$

with $\Delta'(F)$ as given by Eq. (9). Use has been made of the fact that the barrier is sufficiently large, so that transport is in the Boltzmann regime; Eq. (A2) in Ref. 15 can therefore be used to relate n_c to Δ'. Also the expressions for the temperature and field dependence of the mobility, given in Ref. 13, have been used, with the approximation $c_1 = 1.8\times10^{-9} \approx \exp(-2\alpha a) = \exp(-20)$, with $c_2 = 0.42$ and with $f(F)$ a factor that expresses the field dependence of the mobility

$$f(F) \cong \exp\left\{0.44(\hat{\sigma}^{3/2}-2.2)\left[\sqrt{1+0.8\left(\frac{eaF}{\sigma}\right)^2}-1\right]\right\}. \quad (14)$$

For the devices studied, the maximum of the field scale used in Fig. 5 corresponds to $eaF/\sigma \approx 2$. It follows from Eqs. (13) and (14) that at all temperatures considered approximately 30% of the increase of the current density (on a log scale) with the field, observed in Fig. 5, is due to the field dependence of the mobility. The remainder of the effect is due to the energy-barrier lowering with increasing field and to the linear (eaF/σ) factor in Eq. (13).

The dashed-dotted curves in Fig. 5 give the current density as obtained from the 1D continuum injection model by Arkhipov *et al.*[31] Within this model, it is assumed that the current density can be written as an integral over contributions due to hops over variable distances from the electrode to sites at distance $x_0 > a$ and with energy E' with respect to the Fermi level in the electrode. The contribution of each hop is weighed by the escape probability $w_{esc}(x_0)$ out of the image-potential well in which the charge carrier resides after the first hop, toward the bulk of the device

$$J = e\int_a^\infty dx_0\int_{-\infty}^\infty dE'\,W(x_0,E')w_{esc}(x_0)g[E'-e\Delta+ex_0F - e\Phi_{im}(x_0)], \quad (15)$$

with $W(x_0,E)$ the Miller-Abrahams hopping rate given by Eq. (1) and with $w_{esc}(x_0)$ given by

$$w_{esc}(x_0) = \frac{\int_a^{x_0} dx\,\exp\{[-exF+e\Phi_{im}(x)]/(k_BT)\}}{\int_a^\infty dx\,\exp\{[-exF+e\Phi_{im}(x)]/(k_BT)\}}. \quad (16)$$

It may be seen from Fig. 5 that the Arkhipov model yields a field dependence of the current density that is quite close to that obtained from the 1D continuum model (and from the 3D master-equation model), but that the temperature dependence of the current density is much smaller. We tentatively attribute this to the fact that in the expression for the escape probability [Eq. (16)] the effect of disorder is neglected. The percolative nature of the escape process is expected to be more strongly temperature dependent than as predicted by Eq. (16), just as the mobility of disordered materials is more strongly temperature dependent than that of ordered materials. An earlier test of the validity of the Arkhipov model, using Monte Carlo calculations, has not been able to reveal this inadequacy of the model, as the analyses have been carried out only for relatively high temperatures.[32]

V. SUMMARY AND CONCLUSIONS

We have performed a three-dimensional modeling study of the single-carrier transport in devices that consist of a single layer of an organic semiconducting material with a Gaussian distribution of site energies with standard deviation σ, sandwiched in between two metallic electrodes. The voltage-dependent current density was obtained by solving the Pauli master equation corresponding to the related hopping problem, taking the effects of the space charge, the image potential, a finite injection barrier, and the full dependence of the hopping rates on temperature, carrier density, and electric field into account.

The calculations reveal that the current density can be strongly filamentary and that the current filaments become more pronounced with increasing disorder parameter $\hat{\sigma}$

$=\sigma/(k_BT)$, decreasing layer thickness, and increasing injection barrier. Visualizations of the 3D current density show that these filaments become straight near the injecting electrode when the injection barrier is large, for high fields and for strong disorder, as assumed in a 1D master-equation model by Burin and Ratner.[34] In that limit the nonuniformity of the current density is found to give rise to wide distributions of the current density in an ensemble of nanometer-scale devices. The average current density can be much larger than the peak value in the distribution due to the occurrence of a small fraction of devices with extremely high current densities.

A quantitative analysis of the results has been given by making a comparison to the results from a 1D continuum drift-diffusion model, which extends an earlier developed model[25] by including the image-charge effect. The voltage-dependent current-density curves as obtained from both models show a remarkably good agreement (Fig. 1), except for large voltages, disorder parameters, and injection barriers, where the full 3D calculations reveal an enhanced current density. This is attributed to the effects of rare easy pathways for the filamentary current density, as confirmed in Sec. IV from an analysis using the Burin-Ratner model.

We conclude that the 3D master-equation model developed has provided valuable insight in the degree of validity of an also newly developed 1D continuum model. The limitations of the 1D model arise under conditions at which the current density becomes highly nonuniform. However, 1D continuum drift-diffusion models will remain important as a computationally efficient tool for evaluating the materials and device properties of OLED-type devices. In our view, future research toward the improvement of such models should focus on the three following subjects: (i) the explicit consideration of the effect of current filaments, (ii) the development of an approach to the image-potential contribution in the SCLC regime that more consistently takes the space charge near the electrodes into account, and (iii) the possible effects of positional disorder, in particular on the injection-limited current density.

ACKNOWLEDGMENTS

This research was supported by NanoNed, a national nanotechnology program coordinated by the Dutch Ministry of Economic Affairs (J.J.M.v.d.H.), by the Seventh Framework program of the European Community (Grant Agreement No. 213708) (AEVIOM) (R.C. and P.A.B.). The work of M.A.U., G.A.d.W., and R.A.d.G. is part of the research program of the "Stichting voor Fundamenteel Onderzoek der Materie" (FOM) with financial support from the "Nederlandse Organisatie voor Wetenschappelijk Onderzoek" (NWO). The computations were made possible by support from NCF (Dutch National Computer Facilities). We acknowledge Jurgen Rusch for valuable assistance in making the three-dimensional visualizations and Siebe van Mensfoort for useful suggestions about our paper.

*Author to whom correspondence should be addressed; j.j.m.v.d.holst@tue.nl

[1] J. H. Burroughes, D. D. C. Bradley, A. R. Brown, R. N. Marks, K. Mackay, R. H. Friend, P. L. Burns, and A. B. Holmes, Nature (London) **347**, 539 (1990).
[2] C. J. Drury, C. M. J. Mutsaers, C. M. Hart, M. Matters, and D. M. de Leeuw, Appl. Phys. Lett. **73**, 108 (1998).
[3] C. Brabec, V. Dyakonov, J. Parisi, and N. S. Sariciftci, *Organic Photovoltaics: Concepts and Realization* (Springer-Verlag, Berlin, 2003).
[4] L. Pautmeier, R. Richert, and H. Bässler, Synth. Met. **37**, 271 (1990).
[5] H. Bässler, Phys. Status Solidi B **175**, 15 (1993).
[6] Y. N. Gartstein and E. M. Conwell, Chem. Phys. Lett. **245**, 351 (1995).
[7] D. H. Dunlap, P. E. Parris, and V. M. Kenkre, Phys. Rev. Lett. **77**, 542 (1996).
[8] S. V. Novikov, D. H. Dunlap, V. M. Kenkre, P. E. Parris, and A. V. Vannikov, Phys. Rev. Lett. **81**, 4472 (1998).
[9] Z. G. Yu, D. L. Smith, A. Saxena, R. L. Martin, and A. R. Bishop, Phys. Rev. Lett. **84**, 721 (2000).
[10] D. Monroe, Phys. Rev. Lett. **54**, 146 (1985).
[11] M. C. J. M. Vissenberg and M. Matters, Phys. Rev. B **57**, 12964 (1998).
[12] R. Schmechel, Phys. Rev. B **66**, 235206 (2002).
[13] W. F. Pasveer, J. Cottaar, C. Tanase, R. Coehoorn, P. A. Bobbert, P. W. M. Blom, D. M. de Leeuw, and M. A. J. Michels, Phys. Rev. Lett. **94**, 206601 (2005).
[14] C. Tanase, P. W. M. Blom, and D. M. de Leeuw, Phys. Rev. B **70**, 193202 (2004).
[15] R. Coehoorn, W. F. Pasveer, P. A. Bobbert, and M. A. J. Michels, Phys. Rev. B **72**, 155206 (2005).
[16] B. Movaghar and W. Schirmacher, J. Phys. C **14**, 859 (1981).
[17] O. Rubel, S. D. Baranovskii, P. Thomas, and S. Yamasaki, Phys. Rev. B **69**, 014206 (2004).
[18] V. I. Arkhipov, P. Heremans, E. V. Emelianova, G. J. Adriaenssens, and H. Bässler, J. Phys.: Condens. Matter **14**, 9899 (2002).
[19] H. C. F. Martens, I. N. Hulea, I. Romijn, H. B. Brom, W. F. Pasveer, and M. A. J. Michels, Phys, Rev. B **67**, 121203(R) (2003).
[20] Z. G. Yu, D. L. Smith, A. Saxena, R. L. Martin, and A. R. Bishop, Phys. Rev. B **63**, 085202 (2001).
[21] E. Tutiš, I. Batistić, and D. Berner, Phys. Rev. B **70**, 161202(R) (2004).
[22] K. D. Meisel, W. F. Pasveer, J. Cottaar, C. Tanase, R. Coehoorn, P. A. Bobbert, P. W. M. Blom, D. M. de Leeuw, and M. A. J. Michels, Phys. Status Solidi C **3**, 267 (2006).
[23] N. Rappaport, Y. Preezant, and N. Tessler, Phys. Rev. B **76**, 235323 (2007).
[24] J. J. Kwiatkowski, J. Nelson, H. Li, J. L. Bredas, W. Wenzel, and C. Lennartz, Phys. Chem. Chem. Phys. **10**, 1852 (2008).
[25] S. L. M. van Mensfoort and R. Coehoorn, Phys. Rev. B **78**, 085207 (2008).
[26] R. de Levie and H. Moreira, J. Membr. Biol. **9**, 241 (1972).

[27] P. R. Emtage and J. J. O'Dwyer, Phys. Rev. Lett. **16**, 356 (1966).
[28] J. Campbell Scott and G. G. Malliaras, Chem. Phys. Lett. **299**, 115 (1999).
[29] B. Masenelli, D. Berner, M. N. Bussac, F. Nüesch, and L. Zuppiroli, Appl. Phys. Lett. **79**, 4438 (2001).
[30] Y. N. Gartstein and E. M. Conwell, Chem. Phys. Lett. **255**, 93 (1996).
[31] V. I. Arkhipov, E. V. Emelianova, Y. H. Tak, and H. Bässler, J. Appl. Phys. **84**, 848 (1998).
[32] V. I. Arkhipov, U. Wolf, and H. Bässler, Phys. Rev. B **59**, 7514 (1999).
[33] T. van Woudenbergh, P. W. M. Blom, M. C. J. M. Vissenberg, and J. N. Huiberts, Appl. Phys. Lett. **79**, 1697 (2001).
[34] A. L. Burin and M. A. Ratner, J. Chem. Phys. **113**, 3941 (2000).
[35] T. N. Ng, W. R. Silveira, and J. A. Marohn, Phys. Rev. Lett. **98**, 066101 (2007).
[36] A. Miller and E. Abrahams, Phys. Rev. **120**, 745 (1960).
[37] J. G. Simmons, J. Appl. Phys. **34**, 1793 (1963).
[38] Y. Roichman and N. Tessler, Appl. Phys. Lett. **80**, 1948 (2002).